11 Sep 2013

Stabilizing Nanostructured Solid Oxide Fuel Cell Cathode with Atomic Layer Deposition

Yunhui Gong

Diego Palacio

Xueyan Song

Rajankumar L. Patel

et. al. For a complete list of authors, see https://scholarsmine.mst.edu/che_bioeng_facwork/1937

Recommended Citation

Y. Gong et al., "Stabilizing Nanostructured Solid Oxide Fuel Cell Cathode with Atomic Layer Deposition," *Nano Letters*, vol. 13, no. 9, pp. 4340 - 4345, American Chemical Society, Sep 2013.
The definitive version is available at https://doi.org/10.1021/nl402138w

NANO LETTERS

Letter

pubs.acs.org/NanoLett

Stabilizing Nanostructured Solid Oxide Fuel Cell Cathode with Atomic Layer Deposition

Yunhui Gong,[†] Diego Palacio,[‡] Xueyan Song,*[,‡] Rajankumar L. Patel,[§] Xinhua Liang,*[,§] Xuan Zhao,[†] John B. Goodenough,[∥] and Kevin Huang*[,†]

[†]Department of Mechanical Engineering, University of South Carolina, Columbia, South Carolina 29201, United States

[‡]Department of Mechanical and Aerospace Engineering, West Virginia University, Morgantown, West Virginia 26506, United States

[§]Department of Chemical and Biological Engineering, Missouri University of Science and Technology, Rolla, Missouri 65409, United States

[∥]Texas Materials Institute, The University of Texas at Austin, Austin, Texas 78712, United States

Supporting Information

ABSTRACT: We demonstrate that the highly active but unstable nanostructured intermediate-temperature solid oxide fuel cell cathode, $La_{0.6}Sr_{0.4}CoO_{3-\delta}$ (LSCo), can retain its high oxygen reduction reaction (ORR) activity with exceptional stability for 4000 h at 700 °C by overcoating its surfaces with a conformal layer of nanoscale ZrO_2 films through atomic layer deposition (ALD). The benefits from the presence of the nanoscale ALD-ZrO_2 overcoats are remarkable: a factor of 19 and 18 reduction in polarization area-specific resistance and degradation rate over the pristine sample, respectively. The unique multifunctionality of the ALD-derived nanoscaled ZrO_2 overcoats, that is, possessing porosity for O_2 access to LSCo, conducting both electrons and oxide-ions, confining thermal growth of LSCo nanoparticles, and suppressing surface Sr-segregation is deemed the key enabler for the observed stable and active nanostructured cathode.

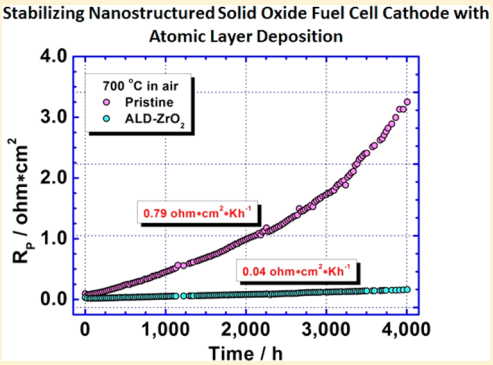

KEYWORDS: *Solid oxide fuel cell, atomic layer deposition, cathode, degradation*

The intermediate-temperature (600−800 °C) solid oxide fuel cell (IT-SOFC) has been actively pursued by the SOFC industry in recent decades because of its great potential to become a commercially viable product. A key to the success of IT-SOFCs is the development of cathodes with high activity and stability. The mixed ion and electron conducting (MIEC), oxygen-deficient perovskites such as $La_{0.6}Sr_{0.4}Fe_{0.8}Co_{0.2}O_{3-\delta}$ (LSCF) and $La_{0.6}Sr_{0.4}CoO_{3-\delta}$ (LSCo) are excellent IT-cathodes owing to their high intrinsic electrocatalytic activity to the oxygen reduction reaction (ORR). However, their high thermal/chemical expansion coefficients and chemical propensity to react with ZrO_2-based electrolytes have presented serious challenges to their practical application. To take full advantage of the high ORR activity without invoking deleterious solid-state reactions and thermal/chemical expansion mismatch within the cell components, LSCo and LSCF are often incorporated as nanoparticles into a preformed porous, ionically conducting scaffold (e.g., electrolyte) at low temperatures through nitrate-solution infiltration methods.[1−5] Such nanostructured, highly active, high-surface-area cathodes promote fast catalysis for the ORR, hence substantially reducing the cathodic polarization, while the ionically conducting backbone simultaneously provides an ionic pathway for charge transfer and structural support for the ORR-active nanoparticles.

However, the primary issue for nanostructured electrodes is the morphological instability caused by agglomeration of nanoparticles under SOFC operating conditions, resulting in a gradual loss of surface area and catalytic activity over time.[1,6−11] The longest stability of nanostructured-electrodes previously demonstrated is less than 500 h even in the temperature range of 650−700 °C,[4,5] and it can become substantially shortened at higher temperatures. Therefore, the retention of thermal stability and catalytic activity of ORR-active nanoparticles under SOFC operating conditions becomes the central requirement for a successful development of nanostructured electrodes for IT-SOFCs. Several mitigating approaches have been reported in the literature, representatives of which include forming the "core-shell" structure,[7] alloying the active metal with more refractory metals,[12] and coimpregnating the active metal with a ceramic-based sintering inhibitor.[8,13] However, so far none of these methods has demonstrated the effectiveness needed to extend the electrode's lifetime to the level of commercial applicability.

Another source of performance degradation arises from the LSCo or LSCF itself. In many laboratory studies where a

Received: June 12, 2013
Revised: July 19, 2013
Published: August 7, 2013

micrometer-sized LSCo or LSCF bulk layer serves as the IT-cathode, pronounced performance degradation over time is still observed.[14−18] Surface chemistry studies assisted by advanced in situ as well as ex situ spectroscopic techniques have provided ample evidence linking the performance degradation in Sr-containing perovskite cathodes, for examples, LSCo, LSCF, and LSM ($La_{0.8}Sr_{0.2}MnO_{3+\delta}$) to the surface segregation of Sr species such as $SrO_{(s)}$,[19−23] a chemical process that is sensitive to temperature, partial pressure of oxygen (pO_2) and electrochemical potential.[18−23] Since the ORR activity of an AMO_3 perovskite as the SOFC cathode depends critically on its surface atomic structure (e.g., electronic configuration) and composition (e.g., cation concentration and oxygen non-stoichiometry),[14−28] a coverage of the passive and insulating $SrO_{(s)}$ layer over the cathode would block the ORR-active sites for charge-transfer. While the phenomenon of surface Sr-enrichment has been actively and systematically studied in the past, a means of alleviating such a detrimental result is surprisingly lacking.

We herein report that the ORR-active but unstable nanostructured cathode, LSCo nanoparticles supported on a porous LSGM ($La_{0.80}Sr_{0.20}Ga_{0.83}Mg_{0.17}O_{3-\delta}$) scaffold, can remarkably retain its performance at 700 °C with exceptional stability for 4000 h by overcoating its surfaces with a conformal layer of nanoscale ZrO_2 films through atomic layer deposition (ALD), an emerging thin-film technology based on the unique binary-sequence and self-limiting reaction chemistry capable of yielding highly conformal and uniform nanoscale films on the surfaces of almost any open bulk geometries.[29−37]

Two different microstructural views taken by TEM of infiltrated LSCo nanoparticles supported on a porous LSGM backbone network are shown in Figure 1. Experimental details

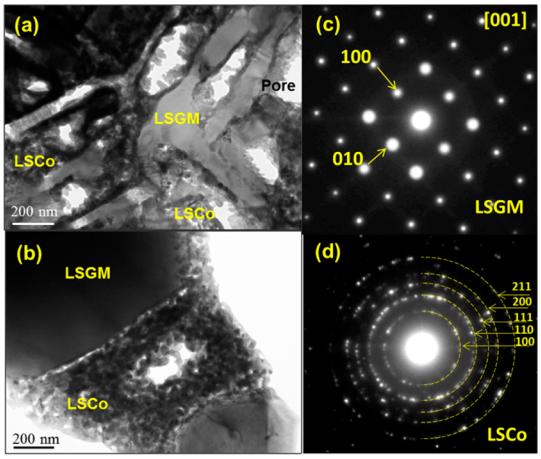

Figure 1. TEM diffraction contrast images showing (a) the porous LSGM backbone infiltrated with LSCo nanoparticles; (b) a magnified view of LSCo nanoparticles; (c) indexing for the diffraction spots from the LSGM backbones; and (d) indexing of the diffraction rings from LSCo grains.

on the preparation of porous LSGM backbones and infiltration of LSCo nanoparticles can be found in the Supporting Information. Several interesting microstructural features are noted in Figure 1. First, in Figure 1a,b the LSGM backbone is well connected and possesses a large quantity of porosity to allow O_2 transport (more microstructural views of the LSGM backbone and infiltrated LSCo nanoparticles can be seen in Figure S1 of the Supporting Information). Second, the LSCo nanoparticles are in the range of 10−20 nm and uniformly distributed along the walls of the LSGM backbone. Local electron diffraction patterns of the backbone LSGM and dispersed LSCo grains shown in Figure 1c,d reveal an oxygen-transport-favorable cubic crystal structure for both LSGM (a = 3.96 Å) and LSCo (a = 3.80 Å), respectively. These unique microstructural and crystal features are a strong support for the observed exceptional ORR-activity and low polarization ASR shown below.

The image of as-synthesized nanoscale ALD-ZrO_2 overcoats (30 ALD cycles) on LSCo nanoparticles is shown in Figure 2.

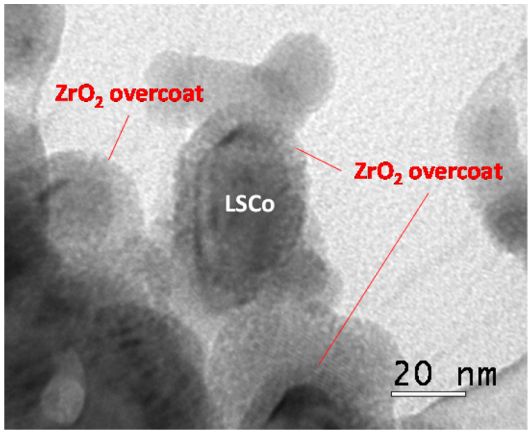

Figure 2. TEM diffraction contrast image showing nanoscale ALD ZrO_2 overcoats (30 ALD cycles) on LSCo nanoparticles.

As expected, the ALD-ZrO_2 overcoats are geometrically conformal around LSCo nanoparticles, which play an important role in confining the thermal growth of underlying LSCo nanoparticles during high-temperature operation. The overall thickness of the overcoat is roughly 5 nm, suggesting a growth rate of 1/6 nm per ALD cycle.

The Nyquist AC impedance complex plots of the pristine and ZrO_2-overcoated nanostructured LSCo cathodes measured at 700 °C are shown in Figure 3 for several selected time

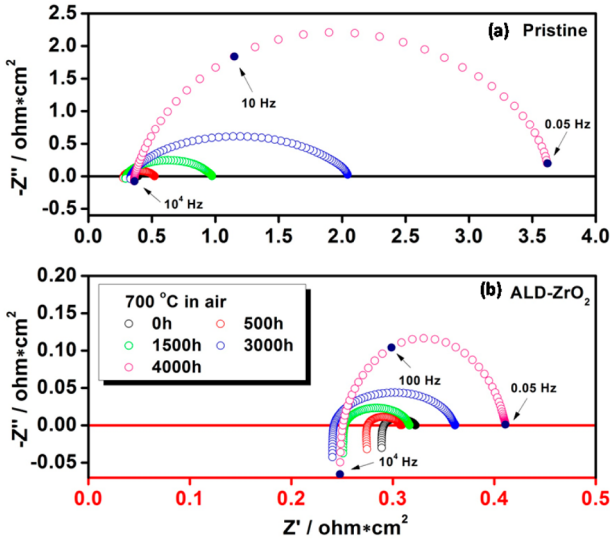

Figure 3. Comparison of EIS spectra between pristine and ALD-ZrO_2 overcoated LSCo-nanoparticle cathodes measured at 700 °C in a flowing air. (a) Pristine sample; (b) ZrO_2-overcoated sample.

dx.doi.org/10.1021/nl402138w | Nano Lett. 2013, 13, 4340−4345

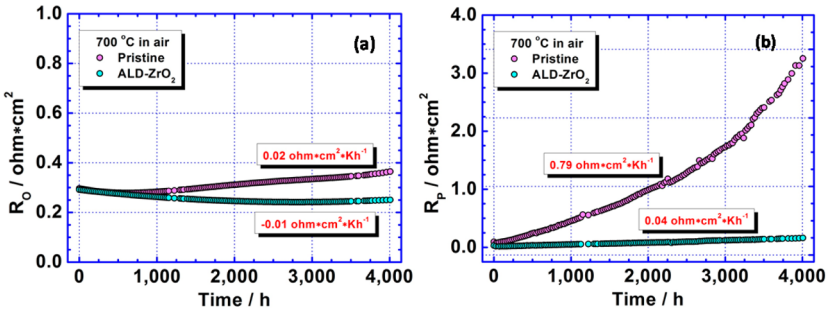

Figure 4. Comparison of long-term stability of pristine and ALD-ZrO_2 overcoated nanostructured LSCo cathodes over 4000 h. (a) R_O and (b) R_P, showing 45% reduction in R_O, 18 times reduction in R_P, and overall 19 times reduction in degradation rate achieved by the ALD-ZrO_2 overcoats.

intervals. The selection of 700 °C as the testing temperature is intentional, primarily aiming to promote a faster agglomeration of LSCo nanoparticles for the long-term stability study. It is evident that the relative values of R_O and R_P varied with time and type of sample. For example, at the beginning of the test the R_P values for both samples are small compared to R_O, which is understandable in that the ohmic resistance from the 200 μm thick LSGM dominates the overall ASR. As the time at temperature increases, the R_P of the pristine sample begins to rise precipitously and eventually becomes the dominant factor for the overall ASR. However, this is not the case for the overcoated sample: R_O is still the largest contributor to the overall ASR for the entire 4000 h testing. This comparison explicitly demonstrates that the overcoated nanostructured cathode possesses a superior ORR-stability. Overall, the magnitude of R_P measured at the first hours for the pristine and overcoated samples is very comparable to those reported in the literature for the similar systems.[38,39]

The R_O and R_P for both cathodes are further plotted in Figure 4 on a continuous time scale over a period of 4000 h. The pristine sample shows a lower R_O in Figure 4a than the overcoated one at the beginning of the test. However, this trend is clearly reversed after ~100 h, and the R_O of the overcoated sample drops below the pristine one with a decreasing trend for another 1,500 h before it finally stabilizes for the remainder of the test. Overall, the pristine sample displays a small but consistent R_O increase with time at a linear rate of 0.02 $\Omega\cdot cm^2$/1000 h, whereas the overcoated sample shows a net decrease in R_O with time at a linear rate of −0.01 $\Omega\cdot cm^2$/1000 h. The combination of the two opposite trends has resulted in the final R_O at the 4000 h marker of the overcoated sample 45% lower than the pristine one. Clearly, the degree of R_O reduction by the ALD-ZrO_2 overcoats is somewhat diluted by the high R_O of the thick LSGM membrane employed in the symmetrical cells. For a thin-film electrolyte cell, the improvement is expected to be even greater.

The most pronounced difference between the two samples is observed on R_P in Figure 4b. After a very small decrease in the first ~24−48 h, R_P of the pristine sample exhibits a strong increase with time over the rest of testing hours at a rate of 0.79 ohm·cm^2/1000 h. In contrast, R_P of the overcoated sample increases at a much smaller rate of 0.04 ohm·cm^2/1000 h, roughly 18 times smaller than the pristine sample. Such a large difference in the growth rate of R_P has led to R_P value of the overcoated sample at the 4000 h marker 19 times smaller than the pristine one. The striking contrast in R_P value of the two samples compellingly illustrates the remarkable effectiveness of ALD-ZrO_2 overcoats in retaining the ORR-activity of nanostructured cathodes. Combining R_O and R_P, the ZrO_2-overcoated nanostructured LSCo cathode exhibits an impressive growth rate (or degradation rate) of total ASR at 0.03 ohm·cm^2/1,000 h.

The time-dependent variations of R_O and R_P for both pristine and overcoated cathodes imply that chemical and structural changes have occurred inside the cathode during the high-temperature operation. While the fast systematic increases in R_O and R_P for the pristine sample can be attributed to the combined effect of surface Sr-enrichment and nanoparticle thermal coarsening, the different trending observed in the overcoated sample means a different mechanism. One likely mechanism is that development of porosity in the ALD ZrO_2-overcoats during thermal exposure due to dehydration and removal of residue carbon in the as-synthesized ZrO_2 overcoats can make O_2 more accessible to the ORR-reactive sites for charge transfer.[30] On the other hand, the cation interdiffusion between Zr and Co is confirmed by EDS analysis showing average concentrations of 5.64 atom % Zr in LSCo and ~13.7 atom % Co in ZrO_2, respectively; the presence of Co in ZrO_2 can introduce mixed oxide-ion and electron conductivity into the ZrO_2 layer, a key attribute for a faster ORR catalysis, and suppress the surface Sr-enrichment. The latter mechanism is further discussed with a new defect-chemistry model as follows.

Another mechanism for the stabilized ORR-activity of nanostructured LSCo cathode can arise from the geometrical confinement of nanoparticles by the ZrO_2-overcoats, thus resulting in resistance to agglomeration and retention of the original high surface area. Otherwise, the nonconfined and free-to-grow LSCo nanoparticles would have been subject to a quick loss of surface area and catalytic activity at elevated temperatures as has been shown in Figure 4b.

If the increase in ASRs of the pristine nanostructured LSCo cathode is indeed associated with the surface Sr-enrichment as widely suggested in the literature, the substantial retention of ASRs (or ORR activity) by nanoscale ZrO_2-overcoats suggest that the ZrO_2-overcoats shall play a vital role in preventing Sr-enrichment from happening. To understand the fundamentals of this process, we herein propose a defect-chemistry model to interpret the mechanisms of degradation caused by the Sr-enrichment and suppression of the Sr-enrichment achieved by the ZrO_2-overcoats.

It is known that the retention of oxygen vacancies, $V_o^{\bullet\bullet}$, in air at the cathode requires operation on a redox couple that is near or pinned at the top of the O-2p band.[40] This condition also provides a large enough admixture of M-3d and O-2p orbitals in the redox couple so that the $(180°\text{-}\phi)$ M-O-M d-orbital interactions are strong enough to give itinerant holes in the M(IV)/M(III) redox couple created by the as-prepared Sr'_{La}.

dx.doi.org/10.1021/nl402138w | Nano Lett. 2013, 13, 4340−4345

From a defect-chemistry perspective, there is a surface reaction (in Kröger-Vink notation)

$$\frac{1}{2}O_2 + V_O^{\bullet\bullet} + 2M_M^{\times} = O_O^{\times} + 2M_M^{\bullet} \quad (1)$$

where $2M_M^{\times}$ and $2M_M^{\bullet}$ represent, respectively, two electrons added to the mixed-valent M(IV)/M(III) redox couple by the introduction of an oxygen vacancy $V_O^{\bullet\bullet}$ and restoration of two holes to the M(IV)/M(III) redox couple by absorption of O_2 at $V_O^{\bullet\bullet}$; $O_O^{\times}$ is a regular lattice oxide ion. Pinning of the Fe(IV)/Fe(III), Co(IV)/Co(III), or Ni(IV)/Ni(III) redox couple at the top of the O-2p bands prevents the surface reaction 1 from being biased completely to the right-hand side in air at the operating temperature T_{op} of the fuel cell. As a result, surface oxygen vacancies are retained in the cathode without eliminating all the mobile holes in the M(IV)/M(III) couple, which makes the oxide a mixed oxide-ion/electronic conductor (MIEC) in air at T_{op}. The MIEC condition optimizes the ORR activity of a SOFC cathode.

As in any metal, the itinerant charge carriers are more concentrated at the surface; holes create a positively charged skin that attracts the lattice-negative Sr'_{La}, which are slowly mobile at T_{op}. The positive surface skin would appear to be the driving force for creating over time a Sr-rich surface layer. Application of the ZrO_2 overcoat introduces an LSCo/ZrO_2 interface. To balance Fermi energy E_F across this interface, $Zr_{Co}^{\bullet}$ are inserted from the overcoat into the cathode in exchange for Co(III) (or $Co_{Co}^{\times}$) from the cathode entering the overcoat. This chemical exchange across the interface creates a negatively charged surface layer at the ZrO_2 side of the junction and a positively charged surface layer at the cathode side. The charge separation created across the junction repels the negatively charged Sr'_{La} from the junction to suppress formation of excess surface Sr'_{La}. The multifunctionality of gas transport, mixed conductivity, confinement of nanoparticles and suppression of Sr-segregation presented by the nanoscale ZrO_2 overcoats is schematically illustrated in Figure 5.

This proposed defect-chemistry model predicts that time at higher temperatures is the condition for surface Sr-enrichment of uncoated cathodes, which is consistent with all experimental observations reported for LSCo and LSCF cathodes.[14−18] On the other hand, electrons introduced into the narrow band of LSCo via the external circuit under load reduces the magnitude of the positive charge of the cathode skin, thereby lowering the migration rate of Sr'_{La} toward the surface and prolonging the operating time before reorganization of the surface structure is induced. It has indeed been observed experimentally that a higher cathodic polarization reduces the rate of Sr-enrichment of the surface.[19]

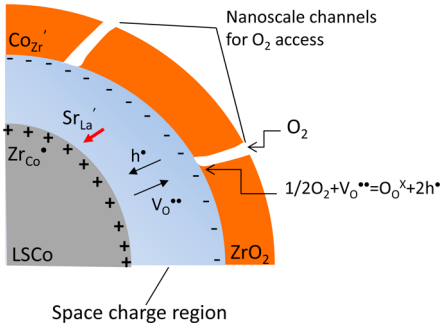

Figure 5. Schematic showing the multifunctionality of gas transport, mixed conductivity, confinement of nanoparticles and suppression of Sr-segregation presented by the nanoscale ZrO_2 overcoated on the surface of nanostructured LSCo cathode. Sr'_{La} is a point defect created by substituting La with Sr while $Zr_{Co}^{\bullet}$ is a point defect created by substituting Co with Zr in LSCo and Co'_{Zr} is a point defect created by substituting Zr with Co in ZrO_2.

As has been pointed out previously,[41] the ORR activity of the LSCo or LSCF cathodes is largely determined by the intermediate-spin (IS) Co(III) or $Co_{Co}^{\times}$ available at a $V_O^{\bullet\bullet}$ on the surface. The occupied $(3z^2\text{-}r^2)$ orbital on the IS Co(III) would be oriented toward a surface $V_O^{\bullet\bullet}$, which also attracts an adsorbed O_2^- molecule followed by an easy electron transfer from the IS Co(III) to create an absorbed $(O_2)^{2-}$ molecule. The coexistence of surface $V_O^{\bullet\bullet}$ and IS Co(III), that is, $Co_{Co}^{\times}$, is enhanced by a shift of equilibrium (1) to the left with surface-Sr enrichment until the surface-Sr enrichment is large enough to create a surface structure instability. However, before the surface structure is destabilized, the shift of equilibrium (1) to the left by increasing the Sr'_{La} concentration at the surface enhances the ORR activity until restructuring of the surface structure sets in. This prediction is consistent with recent studies of LSCo on the surface-Sr segregation[20,42,43] in which the presence of Sr-enriched phases, identified by in situ ambient pressure XPS, was found to promote the oxygen surface exchange rate at low coverage, but reduce the activity at higher coverage.

In summary, the present comparative study of pristine and ALD-ZrO_2 overcoated nanostructured LSCo IT-cathodes explicitly demonstrates the effectiveness of creating a conformal layer of nanoscale ZrO_2 films to retain the ORR activity of the resultant cathodes exposed to air at 700 °C for 4000 h. The ZrO_2 overcoats gradually become porous and mixed conducting after thermal exposure, making it ORR active. With a new defect-chemistry model, the improved ORR-activity retention is also interpreted to be a result of the suppressed Sr-enrichment by an exchange of $Zr_M^{\bullet}$ for Co(III) and the creation of a space charge layer across the cathode/ZrO_2 interface. Furthermore, the geometrical confinement provided by the conformal ZrO_2-overcoats also effectively prevents the LSCo nanoparticles from agglomerating during an extended period of high-temperature operation. Overall, it is the multifunctionality presented by the ALD-derived nanoscaled ZrO_2 overcoats, that is, possessing porosity for O_2 access to LSCo, conducting both electrons and oxide-ions, confining thermal growth of LSCo nanoparticles, and suppressing surface Sr-segregation that enables a stable and active nanostructured cathode.

■ ASSOCIATED CONTENT

Supporting Information

A detailed methods section including preparation of symmetrical impedance cells, ALD coating, electrochemical testing, and TEM examination is provided. This material is available free of charge via the Internet at http://pubs.acs.org.

■ AUTHOR INFORMATION

Corresponding Author

*E-mail: (K.H.) kevin.huang@sc.edu; (X.L.) liangxin@mst.edu; (X.S.) xueyan.song@mail.wvu.edu.

Author Contributions

K.H. proposed the concept of stabilizing active IT-SOFC cathode with ALD-ZrO_2 overcoats and drafted the manuscript. Y.G. and X.Z. prepared electrochemical cells and performed

electrochemical testing. D.P. and X.S. performed HRTEM analysis. R.L.P. and X.L. performed ALD coating of ZrO_2 nanofilms on the cells. J.B.G. created the defect model to interpret the Sr-enrichment process and the role of nanoscale ZrO_2 overcoats played in suppressing the performance detrimental Sr-enrichment.

Notes

The authors declare no competing financial interest.

■ ACKNOWLEDGMENTS

The work is supported by the U.S. Army Research Laboratory and the U.S. Army Research Office under Grant W911NF-10-R-006. J.B.G. thanks the Robert A. Welch Foundation of Houston, Texas for financial support. Special thanks are given to Professor Kenneth Reifsnider of University of South Carolina for reading and providing constructive comments for the manuscript.

■ REFERENCES

(1) Vohs, J. M.; Gorte, R. J. High-Performance SOFC Cathodes Prepared by Infiltration. *Adv. Mater.* **2009**, *21*, 943−956.

(2) Kurokawa, H.; Yang, L. M.; Jacobson, C. P.; De Jonghe, L. C.; Visco, S. J. Y-doped $SrTiO_3$ based sulfur tolerant anode for solid oxide fuel cells. *J. Power Sources* **2007**, *164*, 510−518.

(3) Shah, M.; Barnett, S. A. Solid oxide fuel cell cathodes by infiltration of $La_{0.6}Sr_{0.4}Co_{0.2}Fe_{0.8}O_{3-\delta}$ into Gd-Doped Ceria. *Solid State Ionics* **2008**, *179*, 2059−2064.

(4) Sholklapper, T. Z.; Kurokawa, H.; Jacobson, C. P.; Visco, S. J.; De Jonghe, L. C. Nanostructured solid oxide fuel cell electrodes. *Nano Lett.* **2007**, *7*, 2136−2141.

(5) Sholklapper, T. Z.; Radmilovic, V.; Jacobson, C. P.; Visco, S. J.; De Jonghe, L. C. Synthesis and stability of a nanoparticle-infiltrated solid oxide fuel cell electrode. *Electrochem. Solid-State Lett.* **2007**, *10*, B74−B76.

(6) Tucker, M. C.; Lau, G. Y.; Jacobson, C. P.; DeJonghe, L. C.; Visco, S. J. Performance of metal-supported SOFCs with infiltrated electrodes. *J. Power Sources* **2007**, *171*, 477−482.

(7) Kim, J. S.; et al. Highly Active and Thermally Stable Core-Shell Catalysts for Solid Oxide Fuel Cells. *J. Electrochem. Soc.* **2011**, *158*, B596−B600.

(8) Klemenso, T.; Thyden, K.; Chen, M.; Wang, H.-J. Stability of Ni-yttria stabilized zirconia anodes based on Ni-impregnation. *J. Power Sources* **2010**, *195*, 7295−7301.

(9) Wang, W. S.; Gross, M. D.; Vohs, J. M.; Gorte, R. J. The stability of LSF-YSZ electrodes prepared by infiltration. *J. Electrochem. Soc.* **2007**, *154*, B439−B445.

(10) Shah, M.; Voorhees, P. W.; Barnett, S. A. Time-dependent performance changes in LSCF-infiltrated SOFC cathodes: The role of nano-particle coarsening. *Solid State Ionics* **2011**, *187*, 64−67.

(11) Lee, S.; Miller, N.; Gerdes, K. Long-Term Stability of SOFC Composite Cathode Activated by Electrocatalyst Infiltration. *J. Electrochem. Soc.* **2012**, *159*, F301−F308.

(12) Liang, F. L.; et al. Mn-Stabilised Microstructure and Performance of Pd-impregnated YSZ Cathode for Intermediate Temperature Solid Oxide Fuel Cells. *Fuel Cells* **2009**, *9*, 636−642.

(13) Imanishi, N.; et al. LSM-YSZ Cathode with Infiltrated Cobalt Oxide and Cerium Oxide Nanoparticles. *Fuel Cells* **2009**, *9*, 215−221.

(14) Simner, S. P.; Anderson, M. D.; Engelhard, M. H.; Stevenson, J. W. Degradation mechanisms of La-Sr-Co-Fe-O_3 SOFC cathodes. *Electrochem. Solid-State Lett.* **2006**, *9*, A478−A481.

(15) Mai, A.; Becker, M.; Aseenmacher, W.; Tietz, F.; Hathiramani, D.; Ivers-Tiffée, E.; Stöver, D.; Mader, W. Time-dependent performance of mixed conducting SOFC cathodes. *Solid State Ionics* **2006**, *177*, 1965−1968.

(16) Hjalmarsson, P.; Søgarrd, M.; Mogensen, M. Electrochemical performance and degradation of $(La_{0.6}Sr_{0.4})_{0.99}CoO_{3-\delta}$ as porous SOFC-cathode. *Solid State Ionics* **2008**, *179*, 1422−1426.

(17) Hagen, A.; Liu, Y. L.; Barfod, R.; Hendriksen, P. V. Assessment of the cathode contribution to the degradation of anode-supported solid oxide fuel cells. *J. Electrochem. Soc.* **2008**, *155*, B1047−B1052.

(18) Oh, D.; Gostovic, D.; Wachsman, E. D. Mechanism of $La_{0.6}Sr_{0.4}Co_{0.2}Fe_{0.8}O_3$ cathode degradation. *J. Mater. Res.* **2012**, *27*, 1992−1999.

(19) Finsterbusch, M.; Lussier, A.; Schaefer, J. A.; Idzerda, Y. U. Electrochemically driven cation segregation in the mixed conductor $La_{0.6}Sr_{0.4}Co_{0.2}Fe_{0.8}O_{3-\delta}$. *Solid State Ionics* **2012**, *212*, 77−80.

(20) Crumlin, E. J.; Mutoro, E.; Liu, Z.; Grass, M. E.; Biegalski, M. D.; Lee, Y. L.; Morgan, D.; Christen, H. M.; Bluhm, H.; Yang, S. H. Surface strontium enrichment on highly active perovskite for oxygen electrocatalysis in solid oxide fuel cells. *Energy Environ. Sci* **2012**, *5*, 6081.

(21) Cai, Z.; Kubicek, M.; Fleig, J.; Yildiz, B. Chemical heterogeneities on $La_{0.6}Sr_{0.4}CoO_{3-\delta}$ thin films − correlations to cathode surface activity and stability. *Chem. Mater.* **2012**, *24*, 1116−1127.

(22) Caillol, N.; Pijolat, M.; Siebert, E. Investigation of chemisorbed oxygen, surface, segregation and effect of post treatments on $La_{0.8}Sr_{0.2}MnO_3$ powder and screen-printed layers for solid oxide fuel cell cathodes. *Appl. Surf. Sci.* **2007**, *253*, 4641−4648.

(23) Fisher, T. T.; Fong, D. D.; Eastman, J. A.; Baldo, P. M.; Highland, M. J.; Fuoss, P. H.; Balasubramaniam, K. R.; Meador, J. C.; Salvador, P. A. In-situ characterization of strontium surface segregation in epitaxial $La_{0.7}Sr_{0.3}MnO_3$ thin films as a function of partial pressure. *App. Phys. Lett.* **2008**, *93*, 151904.

(24) Tanaka, H.; Misono, M. Advances in designing perovskite catalysts. *Curr. Opin. Solid State Mater. Sci.* **2001**, *5*, 381.

(25) Serra, J. M.; Vert, V. B.; Betz, M.; Haanappel, V. A. C.; Meulenberg, W. A.; Tietz, F. Screening of A-substitution in the system $A_{0.68}Sr_{0.3}Fe_{0.8}Co_{0.2}O_{3-\delta}$ for SOFC cathodes. *J. Electrochem. Soc.* **2008**, *155*, B207.

(26) Pena, M. A.; Fierro, J. L. G. Chemical structures and performance of perovskite oxides. *Chem. Rev.* **2001**, *101*, 1981.

(27) Shimizu, T. Effect of electronic structure and tolerance factor on Co oxidation activity of perovskite oxides. *Chem. Lett.* **1980**, *1*, 1.

(28) Henrich, V. E. The surfaces of metal oxides. *Rep. Prog. Phys.* **1985**, *48*, 1481.

(29) Stair, P. C. Synthesis of supported catalysts by atomic layer deposition. *Top. Catal.* **2012**, *55*, 93−98.

(30) Elam, J. W.; Dasgupta, N. P.; Prinz, F. B. ALD for clean energy conversion, utilization, and storage. *MRS Bull.* **2011**, *36*, 899−906.

(31) Parsons, G. N.; George, S. M.; Knez, M. Progress and future direction for atomic layer deposition and ALD-based chemistry. *MRS Bull.* **2011**, *36*, 865−871.

(32) George, S. M. Atomic Layer Deposition: A Review. *Chem. Rev.* **2010**, *110*, 111−131.

(33) Ferguson, J. D.; Weimer, A. W.; George, S. M. Optical properties of self-assembled InAs quantum dots grown on GaAs(211)A substrate. *Thin Solid Films* **2000**, *371*, 95.

(34) Ferguson, J. D.; Weimer, A. W.; George, S. M. Atomic layer deposition of SiO_2 films on BN particles using sequential surface reactions. *Chem. Mater.* **2000**, *12*, 3472.

(35) Ott, A. W.; Klaus, J. W.; Johnson, J. M.; George, S. M.; McCarley, K. C.; Way, J. D. Modification of porous alumina membranes using Al_2O_3 atomic layer controlled deposition. *Chem. Mater.* **1997**, *9*, 707.

(36) Cameron, M. A.; Gartland, I.; Smith, P.; Diaz, J. A.; George, S. F. S. M. Atomic Layer Deposition of SiO_2 and TiO_2 in Alumina Tubular Membranes: Pore Reduction and Effect of Surface Species on Gas Transport. *Langmuir* **2000**, *16*, 7435.

(37) Dillon, A. C.; Ott, A. W.; Way, J. D.; George, S. M. Surface chemistry of Al_2O_3 deposition using $Al(CH_3)_3$ and H_2O in a binary reaction sequence. *Surf. Sci.* **1995**, *322*, 230.

(38) Huang, Y.; Ahn, K.; Vohs, J. M.; Gorte, R. J. Characterization of Sr-Doped $LaCoO_3$-YSZ Composites Prepared by Impregnation Methods. *J. Electrochem. Soc.* **2004**, *151*, A1592.

(39) Samson, A. J.; Søgaard, M.; Bonanos, N. Electrodes for Solid Oxide Fuel Cells Based on Infiltration of Co-Based Materials. *Electrochem. Solid-State Lett.* **2012**, *15*, B54−B56.
(40) Goodenough, J. B. Cathode materials: A personal perspective. *J. Power Sources* **2007**, *174*, 996−1000.
(41) Li, Y.; Cheng, J.; Song, J.; Alonso, J. A.; Fernández-Díaz, M. T.; Goodenough, J. B. Characterization of the double perovskite $Ba_2Bi_xSc_{0.2}Co_{1.8-x}O_{6-\delta}$ (x = 0.1, 0.2). *Chem. Mater.* **2012**, *24* (21), 4114−4122.
(42) Mutoro, E.; Crumlin, E. J.; Biegalski, M. D.; Christen, H. M.; Yang, S. H. Enhanced oxygen reduction activity on surface-decorated perovskite thin films for solid oxide fuel cells. *Energy Environ. Sci.* **2011**, *4*, 3689−3696.
(43) Crumlin, E. J.; Mutoro, E.; Ahn, S. J.; La O', G. J.; Leonard, D. N.; Borisevich, A.; Biegalski, M. D.; Christen, H. M.; Yang, S. H. Oxygen Reduction Kinetics Enhancement on a Heterostructured Oxide Surface for Solid Oxide Fuel Cells. *J. Phys. Chem. Lett.* **2010**, *1*, 3149−3155.